J. Phys. B: At. Mol. Opt. Phys. **41** (2008) 025101 (5pp) doi:10.1088/0953-4075/41/2/025101

Evidence of interatomic Coulombic decay in ArKr after Ar 2p Auger decay

Y Morishita[1], N Saito[1], I H Suzuki[1,2], H Fukuzawa[3], X-J Liu[3], K Sakai[3], G Prümper[3], K Ueda[3], H Iwayama[4], K Nagaya[4], M Yao[4], K Kreidi[5], M Schöffler[6], T Jahnke[6], S Schössler[6], R Dörner[6], T Weber[7], J Harries[8] and Y Tamenori[8]

[1] National Institute of Advanced Industrial Science and Technology (AIST), NMIJ, Tsukuba 305-8568, Japan
[2] Photon Factory, Institute of Materials Structure Science, Tsukuba 305-0801, Japan
[3] Institute of Multidisciplinary Research for Advanced Materials, Tohoku University, Sendai 980-8577, Japan
[4] Department of Physics, Kyoto University, 606-8502 Kyoto, Japan
[5] DESY, Notkestrasse 85, 22607 Hamburg, Germany
[6] Goethe-Universität Frankfurt am Main, Max-von-Laue-Str 1, D-60438 Frankfurt, Germany
[7] Lawrence Berkeley National Lab, Berkeley, CA 94720, USA
[8] Japan Synchrotron Radiation Research Institute, Sayo, Hyogo 679-5198, Japan

E-mail: norio.saito@aist.go.jp, ueda@tagen.tohoku.ac.jp

Received 5 October 2007, in final form 20 November 2007
Published 8 January 2008
Online at stacks.iop.org/JPhysB/41/025101

Abstract
We have identified interatomic Coulombic decay (ICD) processes in the ArKr dimer following Ar 2p Auger decay, using momentum-resolved electron–ion–ion coincidence spectroscopy and simultaneously determining the kinetic energy of the ICD electron and the KER between Ar^{2+} and Kr^{+}. We find that the spin-conserved ICD processes in which $Ar^{2+}(3p^{-3}3d)$ ^1P and ^3P decay to $Ar^{2+}(3p^{-2})$ ^1D and ^3P, respectively, ionizing the Kr atom, are significantly stronger than the spin-flip ICD processes in which $Ar^{2+}(3p^{-3}3d)$ ^1P and ^3P decay to $Ar^{2+}(3p^{-2})$ ^3P and ^1D, respectively.

(Some figures in this article are in colour only in the electronic version)

1. Introduction

About a decade ago, Cederbaum *et al* [1] proposed a new mechanism of electronic decay where the environment plays a role. For isolated atoms or molecules with an *innervalence* vacancy Auger decay is often energetically forbidden, but interatomic or intermolecular Coulombic decay (ICD) may occur when another species is in close proximity. Marburger *et al* [2] first observed the ICD process in 2s ionized Ne clusters and later Jahnke *et al* [3] reported clear experimental evidence for ICD in 2s ionized Ne dimers by identifying the process unambiguously using cold-target recoil ion momentum spectroscopy (COLTRIMS) [4, 5]. ICD is relevant to numerous physical, chemical and biological phenomena involving charge and energy transfers from atoms and molecules to their environment, and is thus of significant current interest. Here, we refer to only a small subset of the recent theoretical [6–9] and experimental [10–14] works on ICD.

ICD has also been predicted to take place following Auger decay, as a second step process [15]. Recently, Morishita *et al* [16] investigated ICD in Ar dimers after 2p Auger decay using momentum-resolved electron–ion–ion coincidence spectroscopy (equivalent to COLTRIMS). To our knowledge, however, there has been no experimental report on ICD following Auger decay in hetero-dimers, although these seem to be the clearest prototype system for the investigation of ICD where one atom plays the role of the environment to the other. In the present work, we have extended this observation to hetero-dimers. Namely, we have investigated ICD in ArKr from the states populated by the Auger decay of the Ar 2p inner-shell hole state. In the experiment, each slow electron, either the Ar 2p photoelectron or the ICD electron, is recorded in coincidence with Ar^{2+} and Kr^{+}, and the correlation between

the kinetic energy of the ICD electron and the kinetic energy release (KER) of the two ions is obtained.

2. Experiment

The experiment was carried out at beamline 27SU [17] of SPring-8, using the 26 single-bunches + 2/29 filling mode, which provides a single-bunch separation of 165.2 ns. Radiation polarized linearly in the vertical direction from the figure-8 undulator [18] was monochromatized by the Hettrick-type high-resolution monochromator [19]: the photon bandwidth was set to ∼30 meV at a photon energy of 262.54 eV, which is 13.9 eV and 11.8 eV above the atomic Ar $2p^{-1}{}^2P_{3/2}$ and $^2P_{1/2}$ ionization thresholds.

The Ar–Kr hetero-dimers were produced by expanding a mixture of argon and krypton gases at a flow-rate ratio of 6:1 and a total stagnation pressure of 3.3 atm at room temperature through a pinhole of 50 μm diameter and 0.25 mm thickness. Under these conditions the cluster beam contains a mixture of Ar and Kr monomers, Ar and Kr dimers, Ar–Kr hetero-dimers as well as larger clusters. The cluster beam is directed vertically and crosses the monochromatized radiation.

The momentum-resolved electron–ion–ion coincidence spectroscopy technique is based on recording the electron and ion times-of-flight (TOFs) with multi-hit two-dimensional position sensitive detectors [20–23]. Knowledge of the position and arrival time on the particle detectors, (x, y, t), allows us to extract information on the linear momentum (p_x, p_y, p_z) for each particle. The two TOF spectrometers are placed face to face, and the TOF spectrometer axis is horizontal and perpendicular to both the photon beam and the molecular beam. The TOF spectrometer for the electron is equipped with a hexagonal multi-hit position-sensitive delay-line detector of effective diameter of 120 mm, while that for the ion is of effective diameter 80 mm [24]. A static extraction field and a uniform magnetic field are applied to the spectrometers so that all the electrons and ions ejected to the whole 4π sr solid angle were collected by the detectors.

3. Results and discussion

Figure 1 shows ion–ion coincidence spectra. The x and y coordinates correspond to the TOFs of the first and the second ions of the coincidence pair. The spectrum in the left panel is illustrated using the raw data. The procedure to select only the events $(Ar–Kr)^{3+} \rightarrow Ar^{2+}–Kr^+$ from the raw data is to impose in off-line analysis an acceptance window on the sum of the momentum of the two ions Ar^{2+} and Kr^+, using the momentum conservation law. This selection provides the spectrum in the right panel of figure 1. Ar^{2+} and Kr^+ ions with zero momentum are located at TOFs of 3.27 and 6.70 μs, respectively. One can see clearly the lines corresponding to fragmentation into Ar^{2+}-Kr^+. It is worth noting that this selection rejects not only false coincidences coming from the monomer but also true ion–ion coincidences resulting from the explosion of larger clusters. In the present measurement, the counting rate of the Ar^{2+}–Kr^+ coincidence thus selected relative to the total ion counting rate is 0.05%.

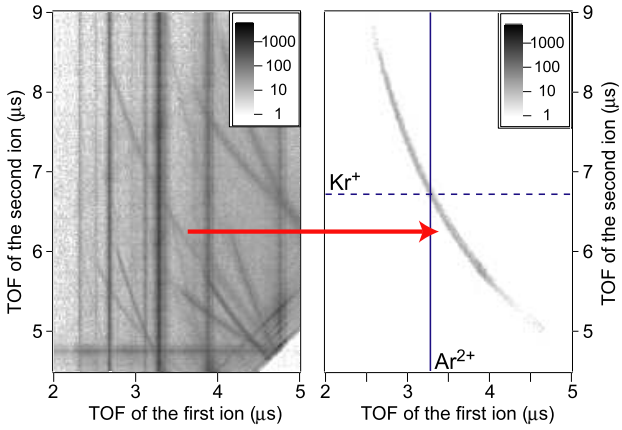

Figure 1. Ion–ion coincidence TOF spectra. The spectrum in the left panel is illustrated using the raw data, without any selections. The spectrum in the right panel is produced using the data selected from the raw data using the condition of the momentum conservation between the Ar^{2+} and Kr^+ ions. The line shows the time-of-flight for zero-momentum Ar^{2+} ions, the dotted line for zero-momentum Kr^+ ions.

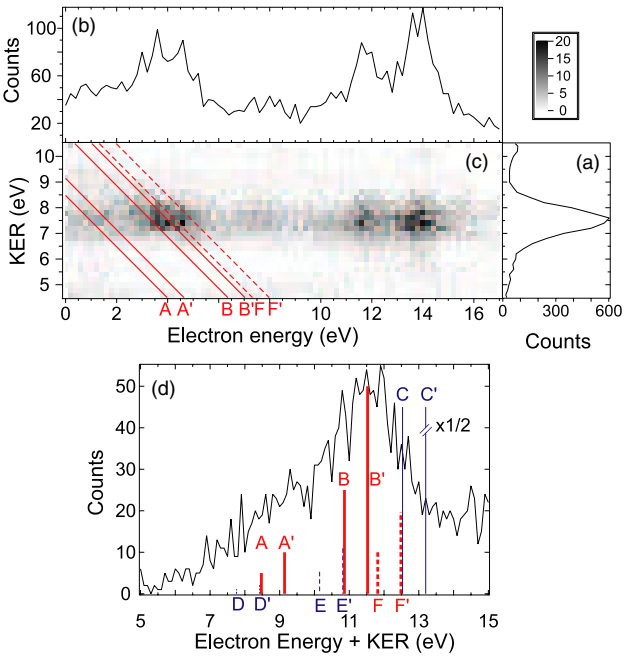

Figure 2. (a) Kinetic energy release (KER) distribution in $(ArKr)^{3+} \rightarrow Ar^{2+}$-$Kr^+$ recorded in coincidence. (b) Energy distribution of the electron ejected from ArKr coincident with the Ar^{2+} and Kr^+ ions. (c) Relationship between the electron energy and the KER. (d) The sum of the electron energy and the KER. The solid lines correspond to the ^{1}P Auger final states (labels of A-C), and the dotted lines the ^{3}P states (labels of D-F). The thick lines A, B, and F, (also shown in (c)), correspond to spin-conserved transitions, and the thin lines C, D, and E correspond to spin-flip transitions.

Figure 2(a) shows the distribution of the KER in $(ArKr)^{3+}$ fragmentation into the Ar^{2+} and Kr^+ ions. The peak energy of 7.47 eV for the KER distribution corresponds to an internuclear distance of 3.85 Å, if one assumes a pure Coulomb explosion and neglects nuclear dynamics. This value is very close to

the bond length of neutral ArKr, 3.88 Å [25], suggesting that Auger decay followed by ICD is faster than the nuclear motion in both the core-ionized state and the Auger final dicationic states of ArKr.

Figure 2(b) shows the energy distribution of electrons coincident with fragmentation into Ar^{2+}–Kr^{+}. The two peaks at 11.8 and 13.9 eV correspond to photoelectrons. A further, broader peak appears at ∼4 eV. This peak corresponds to the ICD electrons as will be discussed below.

Our coincidence measurement for one electron and two ions provides the electron kinetic energy together with the KER between the two ions for each event. The relationship of the electron energy and the KER in the fragmentation into Ar^{2+}–Kr^{+} is shown in figure 2(c). The two islands on the right-hand side are attributed to photoelectrons as described above. The island on the left-hand side corresponds to ICD emission, as discussed below.

In order to make a clear discussion of the ICD processes, the distribution of the sum of the electron kinetic energy and the KER is plotted in figure 2(d). The region shown corresponds to the left-hand side of figure 2(c), and the vertical lines correspond to the energy sums for the ICD transitions, as discussed below.

The energy resolution of our spectrometer depends on the electron and ion energies, and is estimated as follows. The electron kinetic energy resolution is estimated to be 0.4 eV at 4 eV (ICD electrons) and 1.1 eV at 14 eV (photoelectrons). These estimates are derived from the time and position resolutions of the position-sensitive detector, and taking into account that the multiplet components of $Ar^{2+}(2p^{-2})$ are unresolved. The measured full-width at half-maximum of the photoelectron peak at 14 eV is about 1.2 eV, indicating that our estimate is reasonable. The resolution of the ion KER is estimated to be 0.3 eV at a KER of 7.5 eV, estimated from the time and position resolutions of the detector and considering that the Kr isotopes are not resolved. The overall energy resolution for the energy sum in figure 2(d) is thus estimated to be 0.5 eV.

Figure 3 shows a schematic energy level diagram relevant to the ICD after Auger decay. In the independent particle (single-configuration) approximation, the two-vacancy Auger final states of atomic Ar^{2+} are $3p^{-2}$, $3s^{-1}3p^{-1}$, and $3s^{-2}$. In the case of atomic Ar^{2+}, however, the independent particle approximation completely breaks down. For example, the dicationic states at 61.25 and 70.65 eV above the neutral atomic ground state are usually assigned to $3s^{-1}3p^{-1}\,{}^1P$ and $3p^{-3}3d\,{}^1P$, respectively [26, 27]. However, in reality, both configurations $3s^{-1}3p^{-1}$ and $3p^{-3}3d$ are completely mixed in these states [26, 27]. As a result, the Ar atomic Auger transition to the state at 70.65 eV designated as $3p^{-3}3d\,{}^1P$ occurs with significant intensity [27]. This is also the case for the states at 57.56 and 69.94 eV. (Here, we have neglected the energy differences among the triplet states and taken the weighted average of their energies.) Although these states are assigned to $3s^{-1}3p^{-1}\,{}^3P$ and $3p^{-3}3d\,{}^3P$, respectively, these two configurations are also severely mixed. The Auger lines to the satellite state at 69.94 eV also appear with some intensity. The intensity ratio of the Auger transitions to $3p^{-3}3d\,{}^1P$ and to $3p^{-3}3d\,{}^3P$ is roughly 3:1 [27].

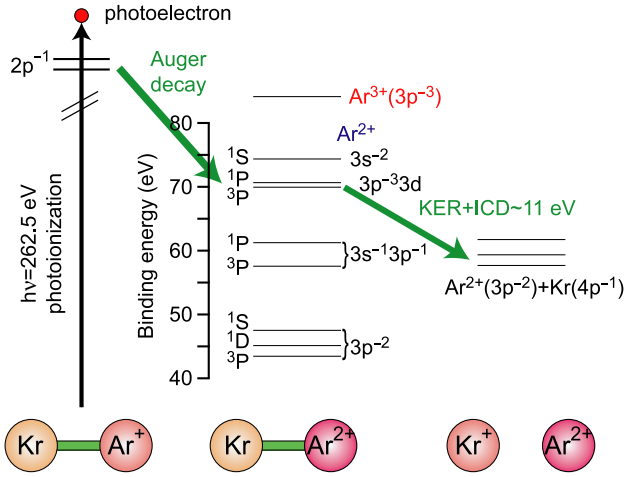

Figure 3. Schematic energy diagram for the states involved in the interatomic Coulombic decay. The triple ionization threshold of atomic Ar is also indicated in the figure.

The triple ionization threshold of atomic Ar (84.12 eV) is higher than all of the Auger final states discussed above, and thus these states are not subject to autoionization in an isolated Ar atom. However, the triple ionization threshold for ArKr is significantly lower since the charge can be delocalized to the two sites. As a result, the states at 70.65 and 69.94 eV, designated as Ar^{2+} $(3p^{-3}3d)$ ^1P and ^3P, respectively, are subject to ICD in the dimer (see figure 3). Although both the Ar^{2+} $(3p^{-3}3d)$ ^1P and ^3P states are populated in atomic Auger decay only via the mixed configuration component $3s^{-1}3p^{-1}$, both the $3p^{-3}3d$ and the $3s^{-1}3p^{-1}$ configurations contribute to ICD: the 3d electron (one of the 3p electrons) in the $3p^{-3}3d$ $(3s^{-1}3p^{-1})$ configuration jumps into the 3p (3s) orbital in the Ar atom by emitting a *virtual* photon, while the Kr atom which absorbed the virtual photon emits a 4p electron as an ICD electron. The possible final states are combinations of the doubly charged states of $Ar^{2+}(3p^{-2})$ and the singly charged states of $Kr^{+}(4p^{-1})$.

The possible ICD channels described above are listed in table 1. The two Auger final states Ar^{2+} $(3p^{-3}3d)$ ^1P and ^3P are the initial states of the ICD and are listed with their energies (relative to the neutral ground state) at the top of the right-hand columns. The ICD final states corresponding to $Ar^{2+}(3p^{-2})$ ^1S, ^1D and ^3P with $Kr^{+}(4p^{-1})$ $^2P_{1/2}$ and $^2P_{3/2}$ are listed with their energies in the first two columns. The possible combinations of the initial and final states of the ICD are labelled A–F and A′–F′ in the table. The prime indicates a $^2P_{3/2}$ final state for Kr^{+}. The listed energies correspond to the sum of the ICD electron energy and the KER, which can be estimated from the listed energies by $E(Ar^{2+}(3p^{-3}3d))-E(Ar^{2+}(3p^{-2}))-E(Kr^{+}(4p^{-1}))$.

The multiplicity of $Ar^{2+}(3p^{-3}3d)$ in the ICD initial states is either singlet or triplet, and the multiplicity of $Ar^{2+}(3p^{-2})$ in the ICD final states is also either singlet or triplet. Let us assume that LSJ coupling is valid in Ar. Then, in the virtual photon exchange picture, the initial Ar^{2+} singlet (triplet) states decay to Ar^{2+} singlet (triplet) states by emitting a virtual photon, which is absorbed by Kr resulting in the emission of

Table 1. Energy levels of the ICD initial states (Auger final states of Ar^{2+} relevant to the ICD) and the ICD final states of Ar^{2+} and Kr^{+} [26]. The labels of A–F correspond to those that appear in figure 2. The values after the labels A–F denote the sum of the ICD electron energy and the kinetic energy release (KER). The parentheses on the labels show that the spin is flipped in Ar^{2+} in the ICD.

ICD final states		ICD initial states	
$Ar^{2+}(3p^{-2})$	$Kr^{+}(4p^{-1})$	$Ar^{2+}(3p^{-3}3d)\ ^1P$ 70.65	$Ar^{2+}(3p^{-3}3d)\ ^3P$ 69.94
^1S 47.51	$^2P_{1/2}$ 14.67	A 8.48	(D 7.76)
^1D 45.13	$^2P_{1/2}$ 14.67	B 10.86	(E 10.15)
^3P 43.46	$^2P_{1/2}$ 14.67	(C 12.53)	F 11.81
^1S 47.51	$^2P_{3/2}$ 14.00	A′ 9.14	(D′ 8.43)
^1D 45.13	$^2P_{3/2}$ 14.00	B′ 11.53	(E′ 10.81)
^3P 43.46	$^2P_{3/2}$ 14.00	(C′ 13.20)	F′ 12.48

the ICD electron: the total spin in Ar^{2+} should be *conserved* in this way. One should however note that ICD can also take place via electron exchange, with a Kr 4p electron filling the Ar^{2+} 3p hole, and an Ar^{2+} 3d electron being ejected as the ICD electron. In this case, the spin may appear to *flip* at the Ar^{2+} site. The labels in parentheses in table 1 indicate these spin-flip ICDs.

The ICD channels listed in table 1 are shown in figure 2(d) by labelled solid and dotted vertical lines. Lines B and B′, corresponding to $E_{\mathrm{sum}} = 10.86$ and 11.53 eV, agree well with the maximum of the energy sum distribution. On the other hand, it is not possible to clearly identify any structure corresponding to line C′. Lines B and B′ correspond to spin-conserved ICDs, whereas lines C and C′ correspond to spin-flip ICDs. Thus, our observation clearly indicates significant suppression of the intensity of spin-flip ICDs in comparison with spin-conserved ICDs. The heights of the thick vertical lines correspond to the products of the relative populations of the ICD initial states as estimated from the Auger intensities (3:1 for ^1P:^3P) and the statistical weights of the spin-conserved ICD final states. The spin-flip ICDs are indicated by thin lines, whose heights are scaled relative to the spin-conserved ICDs by the statistical weights of the final states. It is clear that the spin-conserved ICD channels A, A′, F and F′ also contribute, producing the broad energy-sum distribution of figure 2(d). Again we cannot clearly identify contributions from the spin-flip ICDs to the intensity-sum distributions.

4. Conclusion

We have identified ICD processes from the Auger final states of the ArKr dimer by simultaneously determining the kinetic energy of the ICD electron and the KER between Ar^{2+} and Kr^{+} using momentum-resolved electron–ion–ion coincidence spectroscopy. In the ArKr system the Kr atom can be regarded as the environment for the dicationic Ar^{2+} produced via Ar atomic Auger decay, and this environment opens ICD channels which are energetically forbidden for an isolated Ar atom. We find that spin-conserved ICDs, which can be viewed as energy transfer to the environment (Kr) via virtual photon exchange, are significantly stronger than spin-flip ICDs. We note that ICDs following atomic Auger decay are very general decay channels which lead to the emission of low-energy electrons following inner-shell ionization. These processes are thus relevant to numerous physical, chemical and biological phenomena involving inner-shell vacancies in clusters and other forms of spatially extended atomic and molecular matter, including biomolecules in living cells.

Acknowledgments

The experiment was carried out with the approval of JASRI (2007A1602-NSb-np and 2007A1394-NSb-np). The authors are grateful to S Stoychev, A Kuleff, V Averbukh and LS Cederbaum for discussion on theoretical aspects of this study. The work was supported by grants in aid for scientific research provided by the Japan Society for Promotion of Science (JSPS), the budget for 'Promotion of X-ray Free Electron Laser Research' from the Japanese Ministry of Education, Culture, Sports, Science and Technology, the BMBF and DFG. XJL acknowledges financial support by JSPS. KK acknowledges financial support by DESY and the HGF Initiative and Networking Fund.

References

[1] Cederbaum L S, Zobeley J and Tarantelli F 1997 *Phys. Rev. Lett.* **79** 4778
[2] Marburger S, Kugeler O, Hergenhahn U and Möller T 2003 *Phys. Rev. Lett.* **90** 203401
[3] Jahnke T *et al* 2004 *Phys. Rev. Lett.* **93** 163401
[4] Jahnke T, Weber Th, Osipov T, Landers A L, Jagutzki O, Schmidt L Ph H, Cocke C L, Prior M H, Schmidt-Böcking H and Dörner R 2004 *J. Electron Spectrosc. Relat. Phenom.* **141** 229–38
[5] Ullrich J, Moshammer R, Dorn A, Dörner R, Schmidt L Ph H and Schmidt-Böcking H 2003 *Rep. Prog. Phys.* **66** 1463–545
[6] Santra R, Zobeley J, Cederbaum L S and Moiseyev N 2000 *Phys. Rev. Lett.* **85** 4490
[7] Averbukh V, Müller I B and Cederbaum L S 2004 *Phys. Rev. Lett.* **93** 263002
[8] Averbukh V and Cederbaum L S 2006 *Phys. Rev. Lett.* **96** 053401
[9] Kuleff A I and Cederbaum L S 2007 *Phys. Rev. Lett.* **98** 083201
[10] Öhrwall G *et al* 2004 *Phys. Rev. Lett.* **93** 173401
[11] Bradeanu I L, Flesch R, Meyer M, Jochims H-W and Rühl E 2005 *Eur. Phys. J.* D **36** 173
[12] Aoto T, Ito K, Hikosaka Y, Shigemasa E, Penent F and Lablanquie P 2006 *Phys. Rev. Lett.* **97** 243401
[13] Jahnke T *et al* 2007 *Phys. Rev. Lett.* **99** 153401
[14] Lundwall M *et al* 2007 *J. Chem. Phys.* **126** 214706

[15] Santra R and Cederbaum L S 2003 *Phys. Rev. Lett.* **90** 153401
Santra R and Cederbaum L S 2005 *Phys. Rev. Lett.* **94** 199901(E)
[16] Morishita Y *et al* 2006 *Phys. Rev. Lett.* **96** 243402
[17] Ohashi H, Ishiguro E, Tamenori Y, Kishimoto H, Tanaka M, Irie M, Tanaka T and Ishikawa T 2001 *Nucl. Instrum. Methods* A **467–468** 529
[18] Tanaka T and Kitamura H 1996 *J. Synchrotron Radiat.* **3** 47
[19] Ohashi H *et al* 2001 *Nucl. Instrum. Methods* A **467–468** 533
[20] Fanis A De *et al* 2002 *Phys. Rev. Lett.* **89** 023006
[21] Saito N *et al* 2003 *J. Phys. B: At. Mol. Opt. Phys.* **36** L25
[22] Ueda K, Liu X-J, Prümper G, Fukuzawa H, Morishita Y and Saito N 2007 *J. Electr. Spectrosc. Relat. Phenom.* **155** 113
[23] Saito N, Liu X-J, Morishita Y, Suzuki I H and Ueda K 2007 *J. Electron. Spectrosc. Relat. Phenom.* **156–158** 68
[24] Jagutzki O *et al* 2002 *IEEE Trans. Nucl. Sci.* **49** 2477
[25] Ogilvie J F and Wang F Y H 1993 *J. Mol. Struct.* **291** 313
[26] http://physics.nist.gov/PhysRefData/ASD/levels_form.html
[27] Pulkkinen H, Aksela S, Sairanen O-P, Hiltunen A and Aksela H 1996 *J. Phys. B: At. Mol. Opt. Phys.* **29** 3033